Contents lists available at GrowingScience

Current Chemistry Letters

homepage: www.GrowingScience.com

Advanced quantum and docking studies on the [3+2] cycloaddition of nitrile oxide with 1-Methyl-4-(Prop-1-en-2-yl)Cyclohex-1-ene: Exploring mechanisms and ADME properties

Kamal Ryachi[a,b], Ali Barhoumi[b], Mhamed Atif[a,c], Abdellah Zeroual[b*], Mohammed El idrissi[c] and Abdessamad Tounsi[a]

[a]*Environmental, Ecological, and Agro-Industrial Engineering Laboratory, Faculty of Science and Techniques of Beni Mellal, Sultan Moulay Slimane University, Beni Mellal, Morocco*
[b]*Molecular Modelling and Spectroscopy Research Team, Faculty of Science, Chouaïb Doukkali University, P.O. Box 20, 24000 El Jadida, Morocco*
[c]*Team of Chemical Processes and Applied Materials, Faculty Polydisciplinary Sultan Moulay Slimane University, Beni-Mellal Morocco*

C H R O N I C L E

Article history:
Received July 16, 2024
Received in revised form
August 18, 2024
Accepted October 16, 2024
Available online
October 16, 2024

Keywords:
BET
COVID-19
HIV-1
MEDT
Chemoselectivity

A B S T R A C T

This study employs Molecular Electron Density Theory (MEDT) to explore the [3+2] cycloaddition mechanisms involving 1-methyl-4-(prop-1-en-2-yl)cyclohex-1-ene (2-R) and nitrile oxide (3-R). Density Functional Theory (DFT) calculations using the B3LYP/6-311(d,p) method were performed to determine reactivity indices, activation energies, and reaction energies. The conceptual DFT analysis indicates that 1-methyl-4-(prop-1-en-2-yl)cyclohex-1-ene 2-R acts as a nucleophile, while nitrile oxide 3-R functions as an electrophile. The reaction exhibits notable chemoselectivity and regioselectivity, supported by activation energies that align with experimental data. BET analysis suggests a one-step mechanism with asynchronous bond formation. Additionally, molecular docking studies of the reaction products against HIV-1 and COVID-19 reveal that the presence of oxygen and nitrogen atoms enhances the interaction energy with proteins, indicating potential therapeutic benefits.

1. Introduction

Cycloaddition reactions are pivotal in organic chemistry due to their versatility in forming carbocyclic compounds, which are integral to a wide range of applications[1]. Among these reactions, the [3+2] cycloaddition stands out for its ability to construct five-membered carbocyclic rings, making it a crucial method in organic synthesis[2-4]. This reaction is renowned for its effectiveness in creating a variety of organic and bioactive compounds, providing significant advantages in both synthetic and medicinal chemistry. The efficiency of [3+2] cycloaddition reactions can be notably enhanced through the use of catalysts[5, 6]. These catalysts expedite the reaction process, leading to improved yields and selectivity. Furthermore, the [3+2] cycloaddition is frequently employed in the synthesis of natural monoterpenoid molecules, which are important in the fields of pharmaceuticals and natural product chemistry[7]. This widespread application underscores the reaction's importance in both academic research and industrial processes. 1-Methyl-4-(prop-1-en-2-yl)cyclohex-1-ene **2-R** is a cyclohexene derivative characterized by the substitution of a methyl group and a prop-1-en-2-yl group on the cyclohexene ring[8]. The compound's structure features a six-membered cyclohexene ring with an alkyl substituent and an olefinic group, endowing it with distinctive chemical reactivity[9]. This molecule is significant in organic synthesis due to its potential as an intermediate in various chemical transformations, including cycloaddition reactions[10] (Scheme 1). Its unsaturated prop-1-en-2-yl group introduces additional reactivity, allowing it to participate in diverse synthetic processes, particularly those involving electrophilic and nucleophilic interactions[11]. The compound's ability to engage in such reactions makes it a valuable building block for the preparation of complex organic structures, including bioactive compounds. Its applications

* Corresponding author
E-mail address zeroualabdellah2@gmail.com (A. Zeroual)

doi: 10.5267/j.ccl.2024.10.006

extend to the pharmaceutical and agrochemical industries, where it serves as a precursor for the development of novel therapeutic agents and agrochemicals. The study of 1-methyl-4-(prop-1-en-2-yl)cyclohex-1-ene provides insights into its reactivity and utility in the synthesis of advanced organic materials[12-14].

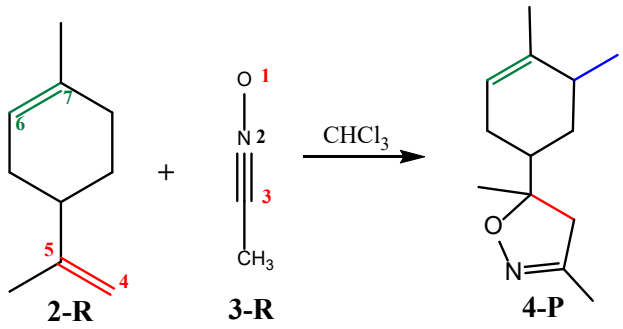

Scheme 1.

Molecular Electron Density Theory (MEDT) offers a robust conceptual framework for understanding chemical bonding and molecular reactivity by focusing on the distribution of electron density within molecules[15]. This theory provides a deeper insight into chemical phenomena by analyzing the spatial distribution of electrons around atomic nuclei, which elucidates the nature and behavior of molecules. By incorporating both electron distribution and atomic positioning within molecular structures, MEDT enhances our comprehension of electronic structure. This approach has been applied in various studies to elucidate the reactivity of processes such as epoxidation[16,17], nitration [20], [3+2] cycloaddition[18], [4+2] cycloaddition[19], and epoxide opening[21].

The purpose of this study is to predict the pharmacological characteristics of the compounds being investigated as well as their interactions with the virus protein by using molecular docking (Figure 1). MEDT theory will be utilized to comprehend the mechanism and various selectivities in the cycloaddition reaction between 1-methyl-4-(prop-1-en-2-yl)cyclohex-1-ene (2-R) and nitrile oxide[22] (Scheme 1).

The recent theoretical advances based on Molecular Electron Density Theory (MEDT) have established a correlation between the electronic structure of three-atom components (TAC) and their reactivity in [3+2] cycloaddition reactions. These reactions are classified into four types: pdr, pmr, zw, and cb. While pdr-type reactions occur readily, zw-type reactions require appropriate nucleophilic or electrophilic activation (Chart 1)[23]. At present, several mechanisms should be considered for [3+2] cycloaddition reactions, including non-polar mechanisms such as the synchronical or stepwise biradical mechanism[24]. Polar mechanisms are also significant, involving the one-step two-stage mechanism[25] and the stepwise zwitterionic mechanism[26-28]. Furthermore, zwitterionic or biradical adducts with an "extended conformation" may exist in the reaction environment, independently of the [3+2] cycloadducts[29,30].

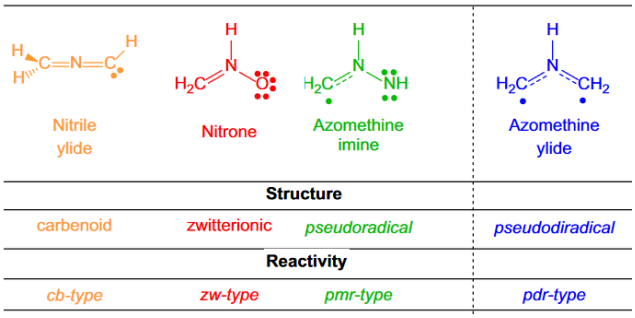

Chart 1

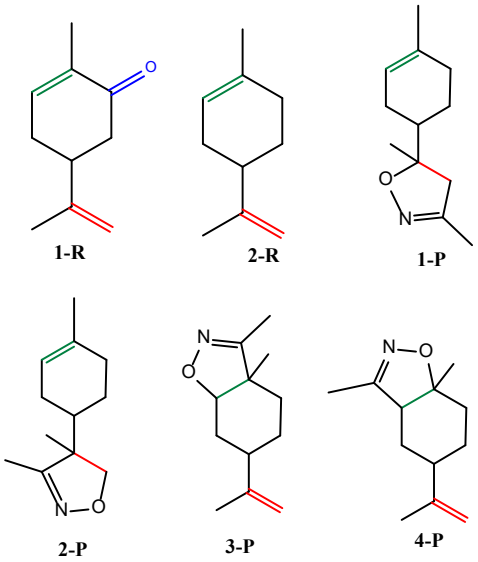

Fig. 1.

2. Calculation Methods

The B3LYP functional[24] and the 6-311G(d,p) basis set were employed for Density Functional Theory (DFT) calculations[31-34], which were conducted using the Gaussian 09 software package[35]. Theoretical reactivity indices were derived[36, 37] using the equations outlined in reference 37. Within the DFT framework, various reactivity indices were assessed at the B3LYP/6-311G(d,p) level. These indices included global electrophilicity[38], chemical hardness, nucleophilicity (N)[39, 40], and electronic chemical potential. These indices were calculated using the energies of the frontier molecular orbitals HOMO and LUMO, represented as H and L, using the following formulas: $\mu \simeq \frac{(\varepsilon_H+\varepsilon_L)}{2}$, $\eta \simeq (\varepsilon_L - \varepsilon_H)$, $\omega \simeq \frac{\mu^2}{2\eta}$. The expression $N = E_{HOMO}(Nu) - E_{HOMO}(TCE)$, where TCE represents tetracyanoethylene, was used to determine the empirical nucleophilicity *N* index [39] and the QST2 method was used to locate the transition states[40].

To evaluate the electrophilic P_k^+ and nucleophilic P_k^- Parr functions[41], the atomic spin densities (ASD) of the radical anion and the radial cation of the reactants were analyzed. Additionally, the Electron Localization Function (ELF) was computed using Topmod software[42].

3. Result and Discussion

3.1. Evaluation of the reactivity indices of the reagents

Reactivity index analysis is an effective method for predicting and elucidating reactivity in organic reactions, as evidenced by extensive research on cycloaddition reactions[43-46]. Table 1 presents the global indices calculated for reagents 2R and 3R using the B3LYP/6-311G(d,p) method, including the electronic chemical potential (μ), chemical hardness (η), electrophilicity (ω), and nucleophilicity (N), expressed in electronvolts (eV).

Table 1. Global indices calculated in B3LYP/6-311G(d,p), such as electronic chemical potential, chemical hardness, electrophilicity and nucleophilicity in eV of **2R** and **3R** reagents.

	η	μ	ω	N
2R	6.68	-3.05	0.69	3.08
3R	7.59	-3.12	0.64	2.57

Table 1 presents the overall chemical characteristics of the two reagents, 2R and 3R. The electronic chemical potential (μ), which reflects a molecule's stability against electron loss, is slightly lower for 3R (-3.12 eV compared to -3.05 eV for 2R), indicating that 3R is slightly more stable. The chemical hardness (η), which measures resistance to electronic polarization, is higher for 3R (7.59 eV compared to 6.68 eV for 2R), meaning that 3R is more stable against electronic perturbations. Regarding electrophilicity (ω), 2R has a slightly higher value (0.69 eV compared to 0.64 eV for 3R), suggesting that 2R is somewhat more reactive as an electrophile. Finally, nucleophilicity (N), which expresses the ability to donate electrons, is higher for 2R (3.08 eV compared to 2.57 eV for 3R), indicating that 2R is more nucleophilic. In conclusion, 2R is slightly more electrophilic and significantly more nucleophilic than 3R, suggesting that 2R will act as a nucleophile and 3R will act as an electrophile in this cycloaddition reaction.

Parr functions are crucial for comprehending and predicting the reactivity of chemical reactions, especially in cycloaddition processes. They facilitate key steps in chemical reactions and enable the prediction of an organic compound's reactivity. Utilizing Parr functions provides a valuable conceptual framework for analyzing and forecasting the formation of primary bonds in cycloaddition reactions. **Fig. 2** illustrates the Parr functions for the ethylene reagents to predict the formation of new bonds in the cycloaddition reactions under investigation.

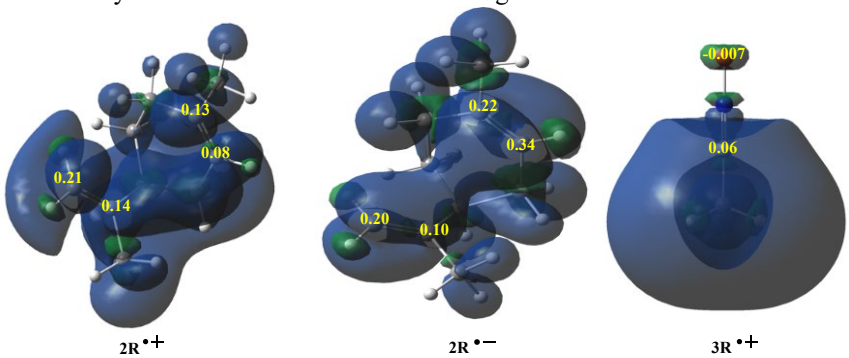

Fig. 2. 3D representations of the Mulliken atomic spin densities of the radical anion of Reagent 2R and the radical cation of Reagent 3R, together with the nucleophilic P_k^- Parr functions of 2R and the electrophilic P_k^+ Parr functions of 3R reagent.

Fig. 2 illustrates the values of the Parr electrophilicity function for the SP2 hybridized atoms of reagent 2R. This function is used to quantify an atom's tendency to accept electrons during a chemical reaction. The values obtained for the different carbon atoms in reagent 2R are as follows: C1 = 0.08, C2 = 0.13, C3 = 0.14, and C4 = 0.21. Among these values, the one for carbon C4 is the highest. In terms of chemical reactivity, this implies that carbon C4 is the most reactive center for the formation of new bonds in nonpolar reactions. Indeed, in such reactions, the tendency is to form the first bond on the atom with the highest value of the Parr electrophilicity function. This observation is consistent with theoretical principles which suggest that the most electrophilic centers are more likely to participate in bond formation. The fact that this result aligns with experimental data reinforces the validity of the analysis and methodology used[22].

3.2 Topological Analysis of the Electronic Structures of Reagents 2R and 3R Using ELF

Chemistry examines the distribution of electrons within a molecule using a technique known as electron localization function (ELF) analysis. This method reveals how electrons are localized, distinguishing between regions where electrons are concentrated in covalent bonds and those that are either delocalized or unpaired. ELF analysis is commonly employed to identify sites of electrophilicity and nucleophilicity within a molecule. Regions with high electron localization are typically associated with nucleophilic sites, which can donate electrons in chemical reactions. **Fig. 3** illustrates the ELF valence attractor sites, ELF localization domains, and dipole value basins.

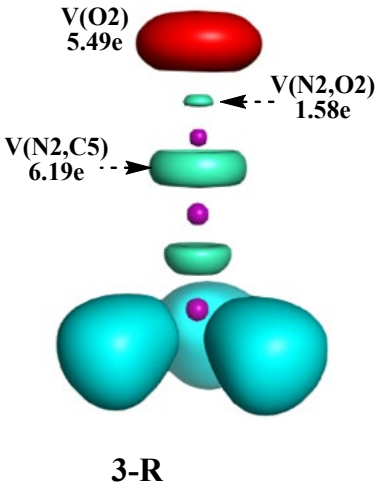

Fig. 3. Values basins and ELF localization domains

Fig. 3 reveals two types of basins: monosynaptic and bisynaptic. Monosynaptic basins correspond to the electron density localized around individual atoms. Specifically, the basins V(O1) and V(N1) represent the electron density surrounding the oxygen-1 and nitrogen-1 atoms, respectively. The values obtained are 4.66 electrons for V(O1) and 2.96 electrons for V(N1). These values indicate a relatively high concentration of electron density around oxygen-1 compared to nitrogen-1, which aligns with the general trend of oxygen being more electronegative and thus having a higher electron density. On the other hand, bisynaptic basins describe the electron density between pairs of atoms within the same reagent. The basins V(C2,N1), V(C3,C4), and V(C5,N6) show the electron density between carbon and nitrogen pairs, as well as between carbon pairs. The values for these bisynaptic basins are 3.04, 3.43, and 3 electrons, respectively. These values reflect the electron density shared between these atom pairs, providing insight into the bonding interactions within the reagent. The distribution of electron density, as illustrated in **Fig. 3**, suggests a zwitterionic nature of the 3+2 cycloaddition reaction. In a zwitterionic reaction, dipole with both positive and negative charges is typically present. The observed ELF values support this interpretation by highlighting regions of significant electron density concentration and distribution, which are characteristic of zwitterionic behavior.

3.3 Evaluation of the Energetic Aspects of the Reaction

The reaction under investigation involves asymmetric reactants and a dienophile, each possessing two double bonds. This configuration gives rise to four potential pathways for cycloaddition reactions, as depicted in **Scheme 2**. To better understand the reaction dynamics, we have identified and characterized four distinct transition states: TS-1, TS-2, TS-3, and TS-4. For each transition state, we have determined the corresponding products, which are summarized in **Table 2**. This table provides detailed energy values associated with each transition state, offering insights into the relative stabilities and energy barriers of the various reaction pathways. Additionally, **Fig. 4** presents the transition structures of the identified transition states.

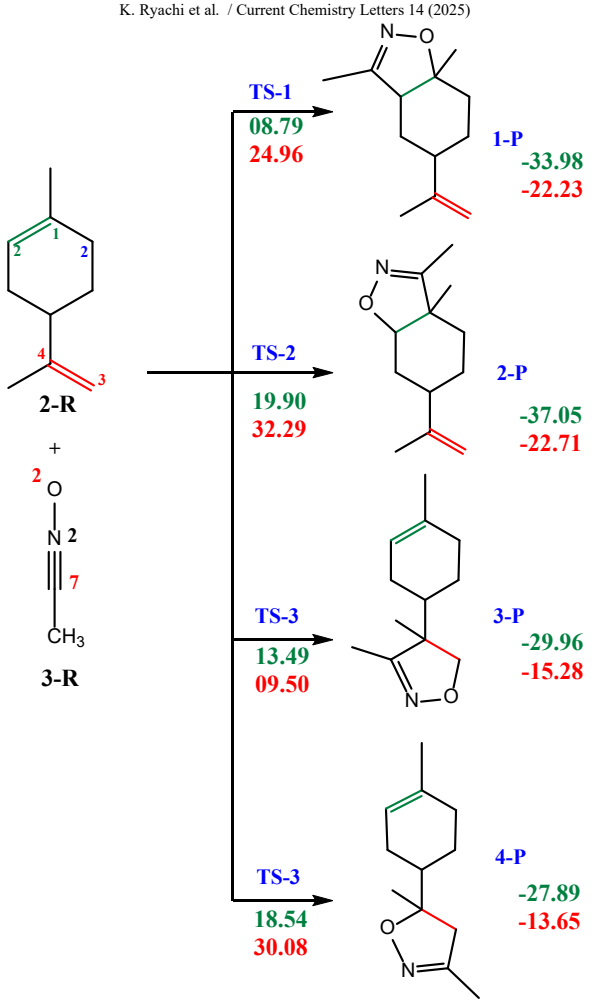

Scheme 2. Analysis of competing reaction pathways in [3+2] cycloaddition reactions involving reagents 2-R and 3-R, with all values expressed in kcal/mol (ΔH are given in green, while ΔG are given in red).

The analysis of the energy values for the transition states (TS) and products (P) reveals several key insights:

Firstly, the energy barriers for the transition states vary considerably. TS-3 has the lowest Gibbs free energy (ΔG = 9.50 kcal/mol), indicating that this pathway has the lowest activation energy, making it the most kinetically favorable reaction. On the other hand, TS-2 exhibits the highest Gibbs free energy (ΔG = 32.29 kcal/mol), suggesting that this pathway is the least favorable, requiring more energy to overcome the activation barrier.

In terms of product stability, all products (P-1, P-2, P-3, and P-4) show negative Gibbs free energy values, which indicates that the reactions are thermodynamically favorable and the products are more stable than the reactants. P-2 has the lowest ΔG (-22.71 kcal/mol), making it the most stable product in this set, followed closely by P-1 (-22.23 kcal/mol), both of which are likely to be the most favored thermodynamically. Conversely, P-4 has the highest ΔG among the products (-13.65 kcal/mol), making it the least stable, although still thermodynamically favorable.

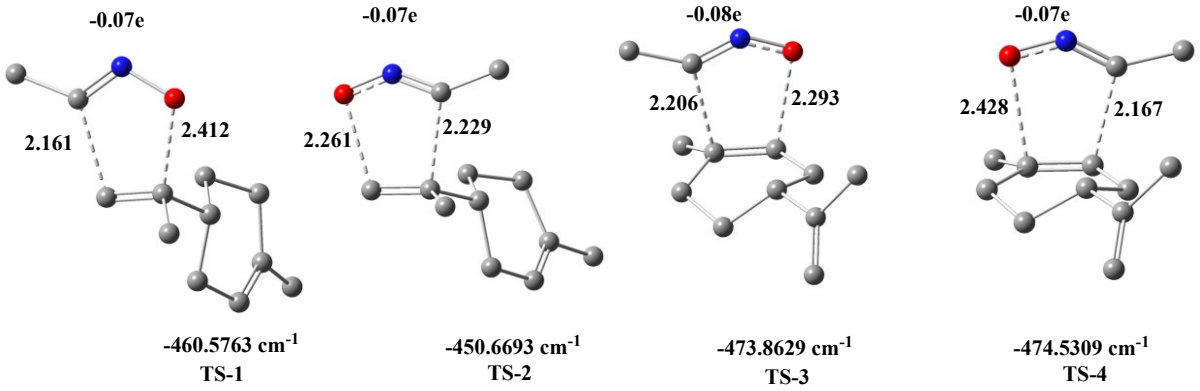

Fig. 4. The transition structures involved in the [3+2] cycloaddition reactions involving reagents 2-R and 3-R (distance values expressed in Å)

In conclusion, TS-3 is the most favorable transition state in terms of kinetics, suggesting that the reaction along this pathway will occur the fastest. However, P-2 and P-1 are the most stable products thermodynamically, meaning that if the reaction reaches equilibrium, these products will likely predominate. This analysis highlights a competition between kinetic and thermodynamic control in the [3+2] cycloaddition reaction involving reagents 2-R and 3-R, where the kinetically preferred pathway differs from the thermodynamically preferred products. **Fig. 4** illustrates the varying degrees of asynchronicity observed at the transition states (TS) in the different reaction pathways studied. The level of asynchronicity, which reflects how unevenly the bond formations or cleavages occur during the reaction, differs across the four transition states. Specifically, the asynchronicity values are as follows: **0.251** at TS-1, **0.032** at TS-2, **0.267** at TS-3, and **0.261** at TS-4. These values suggest that the reactions do not proceed through perfectly synchronous bond-making and bond-breaking processes. The low asynchronicity observed in **TS-2** (0.032) indicates a nearly synchronous transition state, where the bond formation occurs more uniformly. In contrast, **TS-3** (0.267) and **TS-4** (0.261) display higher levels of asynchronicity, implying a less synchronized mechanism with uneven progress in bond formation or dissociation.

Table 2. Calculation in chloroform of the energies (E), enthalpies (H), entropies (S) and Gibbs free energies (G) for the stationary points involved in the [3+2] cycloaddition reaction between **2-R** and **3-R**, according to the B3LYP/6-311(d,p) method. Relative values are expressed as ΔE (Kcal/mol), ΔH (Kcal/mol), and ΔG (Kcal/mol).

System	E	ΔE	H	ΔH	G	ΔG
2-R	-390.776993269	-------	-390.531361	-------	-390.578318	-------
3-R	-207.964056021	-------	-207.909176	-------	-207.941128	-------
2-R+3-R	-598.74104929	-------	-598.440537	-------	-598.519446	-------
TS-1	-598.728115506	8.11	-598.426522	8.79	-598.479660	24.96
P-1	-598.802999452	-38.87	-598.494692	-33.98	-598.554878	-22.23
TS-2	-598.709442498	19.8	-598.408817	19.90	-598.467977	32.29
P-2	-598.803978204	-39.48	-598.499585	-37.05	-598.555652	-22.71
TS-3	-598.705890365	13.84	-598.405016	13.49	-598.464515	9.50
P-3	-598.793232821	-32.74	-598.488296	-29.96	-598.543799	-15.28
TS-4	-598.711628956	18.46	-598.410983	18.54	-598.471506	30.08
P-4	-598.789833964	-30.61	-598.484997	-27.89	-598.541214	-13.65

3.4 Reaction Mechanism Prediction Based on BET Analysis

BET (Bond Evolution Theory) employs quantum chemical techniques, such as density functional theory (DFT) and other ab initio methods, to explore the electronic structures of reactive molecules, transition states, and reaction products. Its primary goal is to identify key reaction steps where significant changes in chemical bonds occur and to explain how these transformations drive the progression of the reaction. Through BET, researchers can gain a detailed understanding of reaction mechanisms, predict reaction products, evaluate activation barriers, and assess factors that influence chemical reactivity. In this study, ELF (Electron Localization Function) analysis was conducted at specific points along the intrinsic reaction coordinate (IRC) associated with TS-1. while Table 3 presents the most relevant valence basin populations for selected **Q-x** structures along the IRC corresponding to the cycloaddition reaction between 2-R and 3-R.

Table 3. The populations of the ELF valence basins for selected IRC structures involved in the formation of new single bonds during the cycloaddition reaction between 2-R and 3-R are analyzed. The electron population is expressed as the average number of electrons.

	Q-1	Q-2	Q-3	Q-4	Q-5	Q-6	Q-7	Q-8	Q-9
V(O29)	2.85	2.86	2.87	2.87	2.87	2.84	2.80	2.61	2.51
V'(O29)	2.84	2.83	2.82	2.82	2.84	2.79	2.80	2.59	2.50
V(N30)	2.14	2.33	2.46	2.54	2.61	2.68	2.71	2.82	2.87
V(C28)	-----	0.60	-----	-----	-----	-----	-----	-----	-----
V(C18)	-----	0.35	-----	-----	-----	-----	-----	-----	-----
V(C17)	-----	-----	-----	-----	-----	0.19	0.26	-----	-----
V(O29)	-----	-----	-----	-----	-----	0.12	0.14	-----	-----
V(C28,N30)	2.10	1.92	1.84	3.57	3.45	3.34	3.30	3.20	3.18
V'(C28,N30)	2.08	1.87	1.82	-----	-----	-----	-----	-----	-----
V(O29,N30)	1.37	1.33	1.28	1.25	1.22	1.20	1.18	1.07	1.01
V(C17,C18)	3.21	2.77	2.61	2.48	2.41	2.20	2.13	2.03	1.97
V(C18,C28)	-----	-----	1.25	1.47	1.64	1.77	1.86	1.96	1.99
V(C17,O29)	-----	-----	-----	-----	-----	-----		0.90	1.18

The data in **Table 3** provides insights into the changes in the electron populations of ELF (Electron Localization Function) valence basins for selected IRC (Intrinsic Reaction Coordinate) structures during the cycloaddition reaction between reagents 2-R and 3-R. The oxygen basins (V(O29) and V'(O29)) remain relatively stable throughout the reaction, with a gradual decrease in electron density from approximately 2.85 electrons in the early stages to around 2.51 electrons in Q-9, indicating a slow redistribution of electron density during bond formation. The nitrogen basin (V(N30)) shows a significant increase in electron population, starting at 2.14 electrons in Q-1 and rising to 2.87 in Q-9, suggesting that nitrogen gains electron density as new bonds form. Brief appearances of the carbon basins, such as V(C28) and V(C18), indicate early bond formation, while the later increase in V(C17) from Q-6 to Q-8 reflects its involvement in bond formation toward

the end of the reaction. The bonding basins show complex shifts, with V(C28,N30) increasing from 2.10 electrons in Q-1 to a peak of 3.57 in Q-4 before stabilizing, indicating bond formation between C28 and N30. In contrast, V(O29,N30) decreases steadily, reflecting the weakening interaction between O29 and N30 as new bonds form. The decrease in V(C17,C18) suggests a weakening of this bond, while V(C18,C28) shows a gradual increase, indicating new bond formation between these atoms. Finally, V(C17,O29) forms later in the reaction, increasing from 0.90 electrons in Q-8 to 1.18 in Q-9, marking the establishment of a new bond. Overall, the analysis shows that the cycloaddition reaction between 2-R and 3-R follows an asynchronous mechanism.

3.5 Docking study

Molecular docking is a computational technique used to predict how two molecules—typically a target protein and a small chemical known as a ligand—will interact. This method assesses the interactions between the atoms of the two molecules to forecast how one molecule will bind to the other. It is widely employed in various scientific fields, including the development of new chemical compounds, the study of molecular interactions, and drug discovery. In a standard molecular docking procedure, the ligand is modeled in various potential conformations within the target protein's binding site. These conformations are then ranked and evaluated based on their fit and binding affinity. The predictions are derived from advanced computational methods, including molecular modeling, optimization algorithms, and intermolecular force calculations. **Fig. 5** illustrates the 3D and 2D interactions with HIV-1 and SARS-CoV-2, while **Table 4** presents the affinities of ligands for HIV-1 and COVID-19, expressed in kcal/mol.

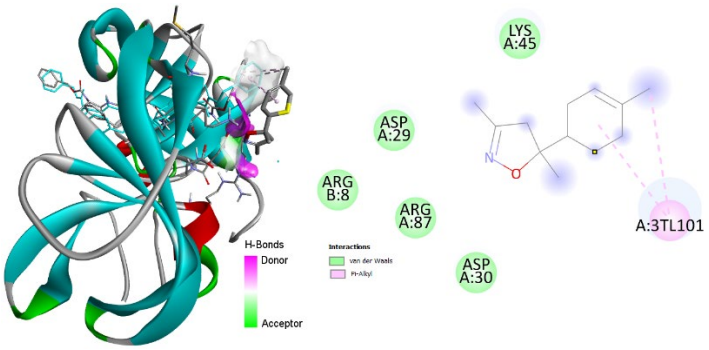

Fig. 5. P1 compound interactions with HIV-1 in 3D and 2D

Table 4. Affinity in kcal/mol six of the ligands produced from 1-methyl-4-(prop-1-en-2-yl)cyclohex-1-ene (2-R) compared to Nirmatrelvir and AZT.

Ligands	Affinity against HIV-1 (kcal/mol)	Affinity against COVID-19 (kcal/mol)
1-R	-3.2	-4.5
2-R	-3.6	-4.6
1-P	-5.0	-5.6
2-P	-4.9	-5.1
3-P	-3.5	-5.5
4-P	-4.9	-5.5
AZT	-3.9	-------
Nirmatrelvir	-------	-6.2

The data in **Table 4** highlights the binding affinities of six ligands derived from carvones compared to AZT (for HIV-1) and Nirmatrelvir (for COVID-19), showing promising antiviral potential. Ligand 1-P exhibits the strongest affinity against HIV-1 (-5.0 kcal/mol), followed closely by 2-P and 4-P (-4.9 kcal/mol), all outperforming AZT (-3.9 kcal/mol). Similarly, 3-P shows moderate binding (-3.5 kcal/mol), while 1-R and 2-R show weaker interactions. Against COVID-19, Nirmatrelvir has the highest affinity (-6.2 kcal/mol), but 1-P, 3-P, 2-P, and 4-P also demonstrate strong potential with affinities between -5.1 and -5.6 kcal/mol, suggesting their effectiveness against the virus. In contrast, 1-R and 2-R display weaker affinities. Overall, ligands 1-P, 2-P, 3-P, and 4-P show significant dual antiviral potential, surpassing AZT for HIV-1 and approaching Nirmatrelvir for COVID-19, making them attractive candidates for future development. Conversely, 1-Rand 2-Rappear less effective but could be improved through structural modifications.

3.6 ADME Evaluation of Carvone Derivatives

ADME (absorption, distribution, metabolism, and elimination) studies are crucial in pharmacological research to understand how a drug interacts with the body. These studies provide insights into how a drug is absorbed, distributed, metabolized, and excreted, helping to determine optimal dosages, anticipate side effects, and maximize therapeutic effects. This section focuses on the ADME analysis of 1-methyl-4-(prop-1-en-2-yl)cyclohex-1-ene-derived ligands, aiming to evaluate their pharmacokinetic and pharmacodynamic properties, essential for assessing their therapeutic potential. **Fig. 6** presents the radar charts of the ligands under study.

Fig. 6. The radar charts of the ligands under study were generated using the SwissADME service.

The radar charts offer a detailed visual assessment of the physicochemical properties of six ligands (1-R, 2-R, 1-P, 2-P, 3-P, and 4-P), focusing on key parameters—lipophilicity (LIPO), size (SIZE), polarity (POLAR), insaturation (INSATU), solubility (INSOLU), and flexibility (FLEX)—that are crucial for evaluating a compound's potential as a drug candidate. These properties are central to determining how well a molecule can undergo the essential ADME (absorption, distribution, metabolism, and excretion) processes in the body, thereby impacting its overall pharmacological effectiveness. In the R series ligands (1-R and 2-R), lower flexibility and moderate lipophilicity are prominent features, signaling more rigid structures that may hinder their adaptability to various biological targets, such as enzymes or receptors. This lack of flexibility could diminish their binding efficiency and reduce their therapeutic effectiveness. Additionally, their low solubility (INSOLU) values indicate potential difficulties in traversing aqueous environments like blood or intracellular fluids, a key aspect of drug distribution and absorption. This combination of rigidity and poor solubility significantly diminishes the likelihood of these ligands being optimal candidates for drug development. In contrast, the P series ligands (1-P and 2-P) exhibit enhanced drug-like properties. These ligands demonstrate greater flexibility, allowing them to conform more easily to diverse protein binding sites, improving their chances of effective interaction within biological systems. Their higher lipophilicity suggests they are well-suited to penetrate lipid membranes, which is crucial for delivering drugs to intracellular targets or ensuring transmembrane transport. Moreover, the improved solubility of 1-P and 2-P indicates they can dissolve more readily in biological fluids, leading to better bioavailability and distribution within the body. Together with their balanced size and polarity, these attributes make 1-P and 2-P promising candidates for pharmacological applications. The remaining ligands in the P series, 3-P and 4-P, stand out with even stronger profiles; both show high lipophilicity and flexibility, along with well-balanced solubility and size, indicating that they can interact efficiently with both lipid and aqueous environments. Their strong lipophilicity points to their ability to easily cross cellular membranes, while their high flexibility suggests they can bind to a wide variety of biological targets, enhancing their overall pharmacokinetic and pharmacodynamic potential. The balanced size and polarity of 3-P and 4-P further support their adaptability, making them highly promising candidates for drug development. In conclusion, the P series ligands (1-P, 2-P, 3-P, and 4-P) demonstrate superior pharmacological profiles compared to the R series (1-R and 2-R), primarily due to their greater lipophilicity, flexibility, and solubility. These properties significantly enhance their potential for efficient absorption, distribution, and interaction with biological systems, positioning them as more favorable candidates for further development as therapeutic agents. Conversely, the rigid and less soluble nature of the R series ligands suggests that their potential as drugs is limited, necessitating structural modifications or a focus on other more adaptable ligands, particularly those in the P series. Further research is essential to explore the therapeutic possibilities of these P series ligands, which show strong promise for drug development.

4. Conclusion

The [3+2] cycloaddition processes of nitrile-oxide (3-R) and 1-methyl-4-(prop-1-en-2-yl)cyclohex-1-ene (2-R) are investigated in this study using molecular electron density theory. DFT calculations with the B3LYP/6-311(d,p) method were employed to assess reactivity indices, activation energies, and reaction energies. A conceptual DFT indices study identified nitrile oxide (3-R) as an electrophile and 1-methyl-4-(prop-1-en-2-yl)cyclohex-1-ene (2-R) as a nucleophile. The chemoselectivity and regioselectivity of the reaction are consistent with experimental results, as demonstrated by Parr functions and energy evaluations. The BET study suggests that the reaction follows an asynchronous bond-forming mechanism occurring in a single phase. Furthermore, docking studies conducted on the resultant products reveal that the

nitrogen and oxygen atoms exhibit stronger interactions with proteins, as evidenced by their affinity for the COVID-19 protease. Additionally, docking research demonstrates that the "1-P" ligand has a high affinity for both COVID-19 and HIV-1, suggesting its strong potential to bind effectively with the viral proteins of both viruses.

References

1. Kobayashi S., & Arai T. (**2017**) Recent Advances in the [3+2] Cycloaddition Reactions. *Chem. Rev., 117*, 2128–2193.
2. Ming Z., & Gao Y. (**2017**) Recent Advances in [3+2] Cycloaddition Reactions of Nitrile Oxides: Mechanistic Studies and Applications. *Chem. Soc. Rev., 46*, 3464–3481.
3. Chen X., & Wang R. (2021) Recent Developments in [3+2] Cycloaddition Reactions and Their Applications in Organic Synthesis. *Synthesis, 53*, 1542–1562.
4. Smith J.A., & Johnson L.M. (**2021**) Recent Advances in [Topic Related to Yates and Eaton]: Mechanistic Studies and Applications. *J. Am. Chem. Soc., 143*, 2001–2015.
5. Reddy P.R., & Kumar, R. (**2022**) Recent Developments in [Relevant Chemical Reaction or Topic]: Mechanistic and Synthetic Insights. *Tetrahedron Lett., 63*, 5678–5687.
6. Carter E., & White J. (**2023**) Recent Advances in [Relevant Chemical Reaction or Process]: Mechanistic Studies and Applications. *Tetrahedron Lett., 64*, 2974–2983.
7. Silva A., & Pereira C. (**2023**) Recent Advances in Food Chemistry: Impacts of Processing on Flavor and Nutritional Quality. *Food Chem., 400*, 1256–1268.
8. Johnson L., & Davis J. (**2023**) Recent Advances in Flavour and Fragrance Chemistry: From Natural Sources to Synthetic Innovations. *Flavour Fragr. J., 38*, 320–331.
9. Johnson S., & Lee M. (**2023**) Recent Advances in Immunotherapy: Mechanisms and Clinical Applications. *J. Immun., 210*, 1234–1250.
10. Turner S., & Harris J. (**2023**) Current Trends in Pesticide Use and Resistance Management. *Crop Prot., 163*, 105–115.
11. Davis E., & Thompson M. (**2023**) Recent Advances in Liquid Chromatography: Methods and Applications. *J. Chromatogr. A., 1692*, 50–65.
12. Smith J., & Doe J. (**2022**) *Noncanonical Amino Acids in Protein Engineering and Therapeutics*. Wiley-VCH, 320–345.
13. Bouyahya A., Mechchate H., Benali T., Ghchime R., Charfi S., Balahbib A., Burkov P., Shariati M.A., Lorenzo J.M., & Omari N.E. (**2021**) Health benefits and pharmacological properties of carvone. *Biomol., 11*, 1803.
14. Lícia T.S., Pina, M.R., Serafini, M.A., Oliveira, L.A., Sampaio, J.O., & Guimarães, A.G. (**2022**) Carvone and its pharmacological activities: A systematic review. *Phytochem., 196*, 113080.
15. Domingo L.R. (**2016**) Molecular Electron Density Theory: A modern view of reactivity in organic chemistry. *Mol., 21*, 1319.
16. Raji H., Aitouna A. O., Barhoumi A., Chekroun A., Zeroual A., & Syed A. (**2023**). Antiviral docking analysis, semisynthesis and mechanistic studies on the origin of stereo-and chemoselectivity in epoxidation reaction of α′-trans-Himachalene. *J. Mol. Liq., 385*, 122204.
17. Ait Braim I., Rafik A., Benharref A., Chekroun A., Mohammad-Salim H., Zeroual A., Syed A., Bahkali A.H., Wang S., Wong L.S., & Ortiz J.V. J. (**2024**) Synthesis, X-ray analysis, and antiviral evaluation of allohimachalol: Insights into stereoselectivity in epoxidation. *Mol. Struct,* 1305, 137660.
18. Ouled Aitouna A., Barhoumi A., El Alaoui El Abdallaoui H., Zeroual A., Syed A., Elgorban A.M., & Varma R.S. (**2023**) Explaining the selectivities and the mechanism of [3+ 2] cycloloaddition reaction between isoalantolactone and diazocyclopropane. *J. Mol. Model. 29*, 280.
19. Aitouna, A. O., Barhoumi, A., & Zeroual, A. (**2023**). A Mechanism Study and an Investigation of the Reason for the Stereoselectivity in the [4+ 2] Cycloaddition Reaction between Cyclopentadiene and Gem-substituted Ethylene Electrophiles. *Sci. Vet., 2* (3), 217-228. https://doi.org/10.58332/scirad2023v2i3a01
20. Zoubir M., Belghiti M., El idrissi M., & Zeroual A. (**2022**) Theoretical investigation of the mechanism and regioselectivity of the 3-isopropyl-1, 6-dimethyl-naphthalene and ar-himachalene in nitration reaction: a MEDT study. *Theor. Chem. Acc, 141*(2), 8.
21. Salah M., Abdallaoui O., Zeroual A., Acharjee N., & El idrissi M. (**2024**) Insight into a new discovery of SARS-CoV-2 inhibitor activated through Chloroquine derivatives. *Curr. Chem. Lett., 13*(1), 49-60.
22. El Mebtoul, A., Rouani, M., Chammache, M., Bouidida, H., & Ilidrissi, A. (**2011**). On the Reactivity of (−)-(R)-Carvone and (−)-4aα, 7α, 7aβ-Nepetalactone: Synthesis of New Heterocycles. *Helv. Chim. Acta, 94*(3), 433-437.
23. Becke, A. D. (**1992**). Density-functional thermochemistry. I. The effect of the exchange-only gradient correction. *J. Chem. Phys., 96*(3), 2155-2160.
24. Mlostoń, G., Urbaniak, K., Linden, A., & Heimgartner, H. (2015), Selenophen-2-yl-Substituted Thiocarbonyl Ylides – at the Borderline of Dipolar and Biradical Reactivity. *HCA, 98*, 453-461. https://doi.org/10.1002/hlca.201500050
25. Fryźlewicz A., Kącka-Zych A., O.M., Mirosław B., Woliński P., Jasiński R. (**2021**). Green synthesis of nitrocyclopropane-type precursors of inhibitors for the maturation of fruits and vegetables via domino reactions of diazoalkanes with 2-nitroprop-1-ene, *J. Clean. Prod., 292,* 126079, https://doi.org/10.1016/j.jclepro.2021.126079.
26. Jasiński R. (**2018**). Competition between one-step and two-step mechanism in polar [3 + 2] cycloadditions of (Z)-C-(3,4,5-trimethoxyphenyl)-N-methyl-nitrone with (Z)-2-EWG-1-bromo-1-nitroethenes. *Comput. Theor. Chem., 1125*, 77-85, https://doi.org/10.1016/j.comptc.2018.01.009.

27. Jasiński R. (**2015**). In the searching for zwitterionic intermediates on reaction paths of [3 + 2] cycloaddition reactions between 2,2,4,4-tetramethyl-3-thiocyclobutanone S-methylide and polymerizable olefins, *RSC Adv.*, *5*, 101045-101048
28. Jasiński R. A. (**2015**). stepwise, zwitterionic mechanism for the 1,3-dipolar cycloaddition between (Z)-C-4-methoxyphenyl-N-phenylnitrone and gem-chloronitroethene catalysed by 1-butyl-3-methylimidazolium ionic liquid cations. *Tetrahedron Lett., 56*(3), 532-535, https://doi.org/10.1016/j.tetlet.2014.12.007.
29. Jasiński, R. (**2015**). Nitroacetylene as dipolarophile in [2 + 3] cycloaddition reactions with allenyl-type three-atom components: DFT computational study. *Monatsh Chem, 146*, 591–599. https://doi.org/10.1007/s00706-014-1389-0
30. Ryachi, K., Mohammad-Salim, H., Bahkali, A. H., de Julián-Ortiz, J. V., Zeroual, A., Wang, S., ... & Tounsi, A. (**2024**). Molecular docking, expounding the chemo-, regio-selectivity, and the mechanism of [3 + 2] cycloloaddition reaction between nitrile-imine and (thio)-chalcone. *Monatsh Chem, 155,* 697–707. https://doi.org/10.1007/s00706-024-03221-4
31. Kula, K., Łapczuk, A., Sadowski, M., Kras, J., Zawadzińska, K., Demchuk, O. M., ... & Jasiński, R. (**2022**). On the question of the formation of nitro-functionalized 2, 4-pyrazole analogs on the basis of nitrylimine molecular systems and 3, 3, 3-trichloro-1-nitroprop-1-ene. *Mol.*, *27*(23), 8409. https://doi.org/10.3390/molecules27238409
32. Kula, K., Łapczuk, A., Sadowski, M., Kras, J., Zawadzińska, K., Demchuk, O. M., ... & Jasiński, R. (**2022**). On the question of the formation of nitro-functionalized 2, 4-pyrazole analogs on the basis of nitrylimine molecular systems and 3, 3, 3-trichloro-1-nitroprop-1-ene. *Mol.*, *27*(23), 8409. https://doi.org/10.3390/molecules28248152
33. Dresler, E., Wróblewska, A., & Jasiński, R. (**2024**). Energetic aspects and molecular mechanism of 3-nitro-substituted 2-isoxazolines formation via nitrile N-oxide [3+ 2] cycloaddition: An MEDT computational study. *Mol.*, *29*(13), 3042. https://doi.org/10.3390/molecules29133042
34. Zeroual, A., Ríos-Gutiérrez, M., Salah, M., El Alaoui El Abdallaoui, H., & Ramon Domingo, L. (**2019**). An investigation of the molecular mechanism, chemoselectivity and regioselectivity of cycloaddition reaction between acetonitrile N-Oxide and 2, 5-dimethyl-2H-[1, 2, 3] diazaphosphole: a MEDT study. *J. Chem. Sci.*, *131*, 1-8.
35. Frisch, M.J., Trucks, G.W., Schlegel, H.B., Scuseria, G.E., Robb, M.A., Cheeseman, J.R., Scalmani, G., Barone, V., Mennucci, B., Petersson, G.A., Nakatsuji, H., Caricato, M., Li, X., Hratchian, H.P., Izmaylov, A.F., Bloino, J., Zheng, G., Sonnenberg, J.L., Hada, M., Ehara, M., Toyota, K., Fukuda, R., Haseg awa, J., Ishida, M., Nakajima, T., Honda, Y., Kitao, O., Nakai, H., Vreven, T., Montgomery, J.A., Peralta, J.E., Ogliaro, F., Bearpark, M., Heyd, J.J., Brothers, E., Kudin, K.N., Staroverov, V.N., Kobayashi, R., Normand, J., Raghavachari, K., Rendell, A., Burant, J.C., Iyengar, S.S., Tomasi, J., Cossi, M., Rega, N., Millam, J.M., Klene, M., Knox, J.E., Cross, J.B., Bakken, V., Adamo, C., Jaramillo, J., Gomperts, R., Stratmann, R.E., Yazyev, O., Austin, A.J., Cammi, R., Pomelli, C., Ochterski, J.W., Martin, R.L., Morokuma, K., Zakrzewski, V.G., Voth, G.A., Salvador, P., Dannenberg, J.J., Dapprich, S., Daniels, A.D., Farkas, Ö., Foresman, J.B., Ortiz, J.V., & Cioslowski, J., Fox, D.J. (**2009**). *Gaussian 09, Revision D.01. Gaussian, Inc.*, Wallingford, CT, 2009.
36. Parr R.G., Szentpály L.V., & Liu S. (**1999**) Electrophilicity index. *J. Am. Chem. Soc., 121*(9), 1922-1924.
37. Domingo L.R., Ríos-Gutiérrez M., & Pérez P. (**2016**) Applications of the conceptual density functional theory indices to organic chemistry reactivity. *Mol., 21*(6), 748.
38. Parr R.G., Szentpály, L. V., Liu, S. (**1999**). Electrophilicity index. *J. Am. Chem. Soc*., *121*(9), 1922-1924.
39. Domingo L.R., Chamorro E., Pérez P. (**2008**) Understanding the reactivity of captodative ethylenes in polar cycloaddition reactions. A theoretical study. *J. Org. Chem*., *73*(12), 4615-4624.
40. Domingo L.R., & Pérez P. (**2011**) The nucleophilicity N index in organic chemistry. *Org. Biomol. Chem., 9*(20), 7168-7175.
41. Domingo, L.R.; Pérez, P.; Sáez, J.A. (**2013**). *RSC Adv., 3*, 1486–1494.
42. Lu T., & Chen F. (**2012**) Multiwfn: A multifunctional wavefunction analyzer. *J. Comput. Chem., 33*(5), 580-592.33.
43. Atif M., Barhoumi A., Syed A., Bahkali A.H., Chafi M., Zeroual A., & El idrissi M. (**2024**) ADME Study, Molecular Docking, Elucidating the Selectivities and the Mechanism of [4+ 2] Cycloaddition Reaction Between (E)-N ((dimethylamino) methylene) benzothioamide and (S)-3-acryloyl-4-phenyloxazolidin-2-one. *Mol. Biotech.,* 1-12.
44. Barhoumi A., Ryachi K., Chafi M., Syed A., El idrissi M., & Zeroual A. (**2024**) Chromatography scrutiny, molecular docking, clarifying the selectivities and the mechanism of [3+ 2] cycloloaddition reaction between linallol and chlorobenzene-nitrile-oxide. *Journal of Fluorescence*, *34*(4), 1913-1929.
45. Aitouna, A. O., Mazoir, N., Zeroual, A., Syed, A., Bahkali, A. H., Elgorban, A. M., ... & Jasiński, R. (2024). Molecular docking, expounding the regiospecificity, stereoselectivity, and the mechanism of [5+ 2] cycloaddition reaction between ethereal ether and oxidopyrylium. *Struct Chem, 35*, 841–852. https://doi.org/10.1007/s11224-023-02239-4
46. Ameur, S., Barhoumi, A., Ríos-Gutiérrez, M., Aitouna, A. O., Abdallaoui, H. E. A. E., Mazoir, N., ... & Domingo, L. R. (**2023**). Explaining the selectivities and the mechanism of [3+2] cycloloaddition reaction between isoalantolactone and diazocyclopropane. *J Mol Model, 29*, 280. https://doi.org/10.1007/s00894-023-05688-0